Article

Fe3C Decorated Folic Acid-Derived Graphene-Like Carbon as Polysulfide Catalyst for High-Performance Lithium-Sulfur Battery

Zenghui Lin , Junan Feng , Wendong Liu , Lu Yin , Wanyang Chen , Chuan Shi , Jianjun Song *

Posted Date: 10 April 2023

doi: 10.20944/preprints202304.0149.v1

Keywords: lithium-sulfur batteries; Fe3C; 2D materials; shuttle effect; catalyst

Article

Fe_3C Decorated Folic Acid-Derived Graphene-like Carbon as Polysulfide Catalyst for High-Performance Lithium-Sulfur Battery

Zenghui Lin †, Junan Feng †, Wendong Liu, Lu Yin, Wanyang Chen, Chuan Shi and Jianjun Song *

College of Physics, Qingdao University, Qingdao 266071, Shandong, China

* Correspondence: jianjun.song@qdu.edu.cn

† These authors contributed equally to this work.

Abstract: Lithium-sulfur (Li-S) battery has been regarded as an important candidate for the next-generation energy storage system due to its high theoretical capacity (1675 mAh g^{-1}) and high energy density (2600 Wh kg^{-1}). However, the shuttle effect of polysulfide seriously affects the cycling stability of the Li-S battery. Here, a novel Fe_3C decorated folic acid-derived graphene-like N-doped carbon sheet (Fe_3C@N-CS) was successfully prepared as the polysulfide catalyst to modify the separator of Li-S battery. The porous layered structures can successfully capture polysulfide as a physical barrier, and the encapsulated Fe_3C catalyst can effectively trap and catalyze the conversion of polysulfide, thus accelerating the redox reaction kinetics. Together with the highly conductive networks, the cell with Fe_3C@N-CS modified separator evinces superior cycling stability with 0.06% capacity decay per cycle at 1 C rate over 500 cycles and excellent specific capacity with an initial capacity of 1260 mAh g^{-1} at 0.2 C. Besides, at a high sulfur loading of 4.0 mg cm^{-2}, the batteries also express superb cycle stability and rate performance.

Keywords: lithium-sulfur batteries; Fe_3C; 2D materials; shuttle effect; catalyst

1. Introduction

The development of modern energy storage systems is undoubtedly a consequential part of the implementation of carbon-neutral strategies in response to the current environmental situation. Lithium-sulfur (Li-S) batteries are one of the most promising expected candidates due to their high energy density (2600 Wh kg^{-1}) and high theoretical capacity (1675 mAh g^{-1})[1,2]. Additionally, sulfur is extremely rich in the earth, nonpoisonous, and eco-friendly [3]. Nevertheless, there are still obstructs in the way of practical commercial application. (i) Sulfur and Li_2S have poor electrical conductivity and the insulating properties render it more difficult to transport ions and electrons; (ii) the cathode will be seriously damaged by the significant volume expansion due to the density difference between sulfur and Li_2S. (iii) The intermediate polysulfides (LiPSs) dissolving in the organic electrolyte will shuttle between the anode and cathode during the reaction process, and this undesirable shuttle effect is not conducive to the full utilization of active material sulfur [4]. This undesirable irreversible side reaction is not beneficial to the maximum utilization of active material sulfur. Moreover, the sluggish conversion kinetics between interface redox kinetics from LiPSs to Li_2S results in a disappointing decay rate of capacity and electrochemical polarization [5].

To solve the above problems, most research focused on the design of the functional sulfur host [6,7], appropriate separator modification [8,9], and electrolyte optimization [10,11]. Among them, modifying separator is a facile strategy to seek a good cycle lifespan of Li-S batteries, and the ideal separators can effectively fix the LiPSs on the side of the cathode to prevent them from reacting with the lithium anode [12,13]. Simultaneously, the functional layer can also serve as the second current collector to ensure the fast transmission of electrons and act as a storage for LiPSs. Among the various adjustments made to the separator, carbon materials are a major focus due to the high electrical

 doi:10.20944/preprints202304.0149.v1

conductivity and the enhanced wettability of electrolytes [14]. Carbon materials, such as conductive carbon nanotubes (CNTs) [15], porous carbon, and carbon nanofiber (CNFs) [16], can effectively reduce the internal interface impedance and charge transfer resistance, improve the Li^+ diffusion kinetics [17]. However, single non-polar carbon material modified separator cannot fully inhibit the shuttle effect relying solely on weak physical adsorption or electrostatic interaction [18]. Polar materials, such as transition metal compounds, produce robust polar chemical interaction on LiPSs and can catalyze the conversion of LiPSs to increase the reaction kinetics of Li-S chemistry [19]. Therefore, the reasonable combination of polar metal oxides, carbides, nitrides, and sulfides with carbon-based materials has shown outstanding properties and become a popular choice in the field of sulfur host design or separator modification of Li-S batteries [20–23]. Fe_3C with the advantages of low price, simple preparation, high conductivity, strong polarity, and remarkable electrochemical catalysis ability make it excellent in the field of LiPSs catalysis. Li et al. synthesized a Janus electrode comprising Fe_3C nanoparticles as active catalytic sites, and the electrode displays synergistic dual adsorption–electrocatalysis function, which can assuage shuttle effect by facilitating the kinetics of redox reactions from the soluble LiPSs to the insoluble LiPSs efficiently [24].

Two-dimensional (2D) materials, such as graphene (GN) and MXene, are seen as a high-quality option for electrochemical energy storage study [25–27], due to excellent ductility, high specific surface area, and exceptional electrical conductivity [28]. Besides, the unique 2D structure can not only provide a great quantity of ion transport channels in the electrochemical kinetics process but also act as a physical barrier for LiPSs. Therefore, it will be highly promising to compound Fe_3C with 2D material GN to achieve the dual physical/chemical adsorption of polysulfide and enhanced redox reaction kinetics.

In this work, we prepared a novel Fe_3C decorated folic acid-derived GN-like N-doped carbon sheet (Fe_3C@N-CS) as the LiPSs catalyst to modify the separator of Li-S batteries. After the hydrothermal method, freeze-drying, and calcination process, the folic acid produces a GN-like structure with interconnected porous lamellar structures with high specific surface area to ensure generous ion migration channels (Figure 1). More importantly, the barrier produced by self-inter-stacking can also serve as a physical barrier to enhance the efficiency of LiPSs capture. The well-dispersed polar Fe_3C nanoparticles on the nanosheet assure abundant chemical adsorption and active catalytic sites to enhance the reaction kinetics of the LiPSs by catalyzing the redox conversion. Profiting from the synergy efficiency of chemisorption and catalytic properties of Fe_3C and the physisorption of highly conductive 2D carbon nanosheets, the Li-S batteries with Fe_3C@N-CS modified separators demonstrated brilliant specific capacity with an excellent capacity of 1260 mAh g^{-1} at 0.2 C and outstanding cycling stability with 0.06% capacity decay per cycle at 1 C over 500 cycles. Even at a high sulfur loading of 4.0 mg cm^{-2}, the batteries still accomplish exceptional cycle stability and rate performance.

Preprints (www.preprints.org) | NOT PEER-REVIEWED | Posted: 10 April 2023 doi:10.20944/preprints202304.0149.v1

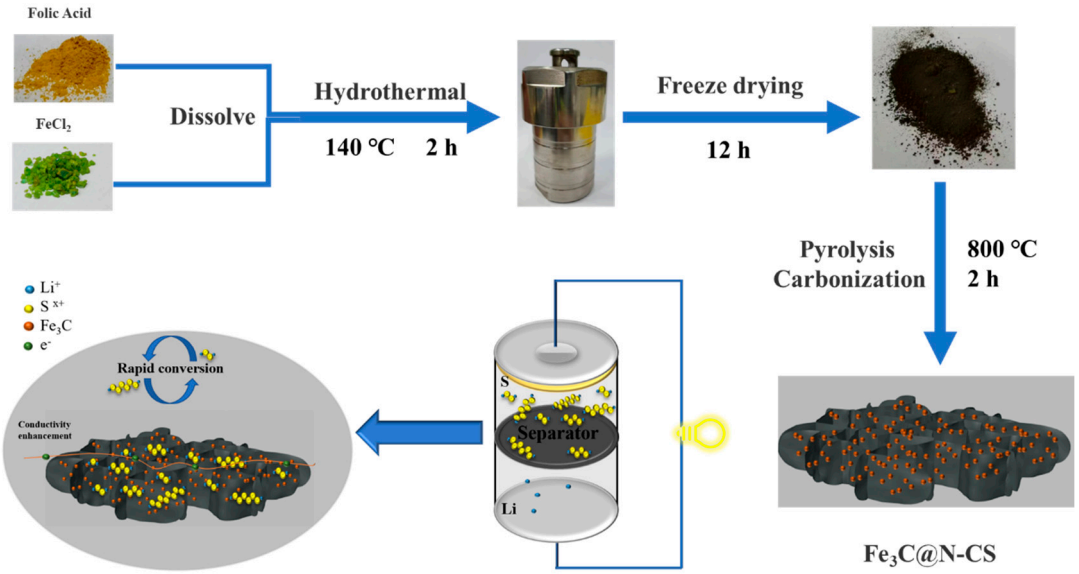

Figure 1. Schematic diagram illustration of the fabrication process of Fe_3C@N-CS and the LiPSs conversion process on the surface of Fe_3C@N-CS.

2. Materials and Methods

2.1. Preparation of Fe_3C@N-CS

Typically, the $FeCl_2 \cdot 4H_2O$ (200 mg) and folic acid (220 mg) is dissolved into a mixture of deionized water (5.5 ml) and anhydrous ethanol (8 ml). Then, the mixed solution was transferred to the autoclave for a solvothermal reaction at a temperature of 140 °C for two hours. Afterward, the solution is centrifuged with deionized water three times, and freeze-dried for ten hours after being frozen overnight. The dried precursor powder is placed in a ceramic boat held in an argon-filled tube furnace and heated to 800 °C with a heating rate of 5 °C min^{-1} and then held for 2 hours to obtain a black powder, marked as Fe_3C@N-CS. N-CS is produced by the same process but without the addition of Fe source.

2.2. The fabrication of Fe_3C@N-CS modified separator

A homogenous slurry consisting of Fe_3C@N-CS and polyvinylidene difluoride (PVDF) with a mass ratio of 5:1 in N-methyl-2-pyrrolidone solvent was uniformly pasted onto the standard PP separator and dried under vacuum at 60 °C for 12 hours. The thickness of the modified diaphragm is approximately 7.63 μm. The separator is cut into discs with a diameter of 19 mm.

2.3. Synthesis of lithium Li_2S_6 solution

Li_2S_6 solution is prepared by adding Li_2S and S powders into the solvent containing 1,2-dimethoxyethane and 1,3-dioxolane with a volume ratio of 1:1 and vigorously stirred for 48 hours in the glovebox at 60 °C. The mole ratio of Li_2S and S is 1:5.

2.4. Electrochemical measures

CR-2032 typed coin cells are assembled with a sulfur cathode (S/CB composites with S content of 70% prepared by a melt-diffusion method), modified separator, electrolyte, and lithium anode in a glove box under an argon atmosphere. ($H_2O \leq 0.01$ ppm, $O_2 \leq 0.01$ ppm). The electrolyte is 1 M lithium bis(trifluoromethane sulfonimide) (LiTFSI) in a mixed solvent of DME/DOL (1: 1, v/v) with 0.1 M $LiNO_3$ as additives. The electrochemical workstation (CHI 760e) is applied to analyze cyclic voltammetry (CV) curves at a working voltage from 1.7 to 2.8 V and a scan rate of 0.1~0.6 mV s^{-1}). Electrochemical impedance spectroscopy (EIS) (1 mHz to 100 kHz and an applied amplitude of 5

Preprints (www.preprints.org) | NOT PEER-REVIEWED | Posted: 10 April 2023 doi:10.20944/preprints202304.0149.v1

mV). The electrochemical information is reported on NEWARE battery measurement system at indoor temperature, and the voltage range is 1.7~2.8 V.

2.5. Material characterization

The XRD (Cu Ka radiation with k = 1.5405 Å) was conducted to investigate phase information of materials in the angle range of 5 ° to 80 °. The SEM (Nova Nano SEM450, 15K eV) and the structure and morphologies of the materials were analyzed by TEM (JEOL JEM 2100F). The XPS was used on ESCALAB250 to detect the chemical composition of samples. HRTEM and attached EDS equipment (Oxford Instruments and EDAX) were employed to analyze the structure and elemental distribution of the materials.

3. Results and discussion

The microstructure of samples is observed by scanning electron microscope (SEM). Untreated folic acid shows the agglomeration morphology at the micron level (Figure S1a,b). After the calcination, the folic acid-derived carbon exhibits two-dimensional carbon nanosheet characteristics as well as GN-like layering and wrinkle structure (Figure 2a and Figure S2). The SEM images of Fe_3C@N-CS (Figure 2b,c) demonstrate that the crinkled and lamellar microstructure is perfectly inherited, and the surface of the lamellar sheet becomes rougher. At the same observation scale, the Fe_3C@N-CS lamellar structure with a unique interconnected porous structure provides more active site exposure as well as an increased contact interface with LiPSs (Figure S3).

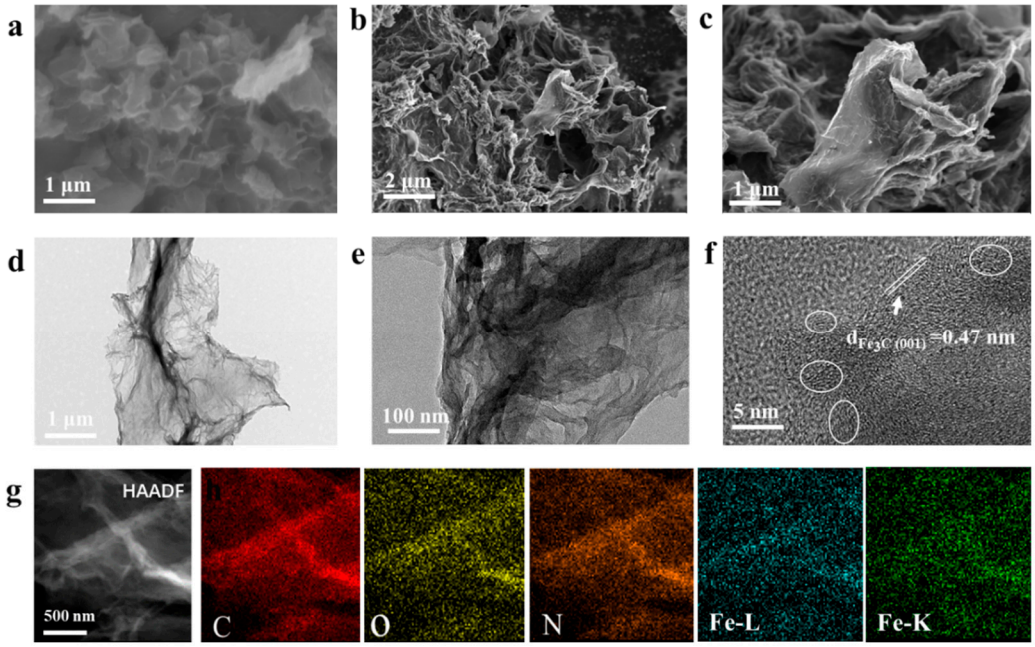

Figure 2. SEM images of N-CS (a) and Fe_3C@N-CS (b, c), TEM images of Fe_3C@N-CS (d, e), HR-TEM image of Fe_3C@N-CS(f). STEM-HADDF of Fe_3C@N-CS and elemental mapping image of C, O, N, Fe-L, and Fe-K in a selected region of Fe_3C@N-CS (g).

The transmission electron microscope (TEM) images (Figure 2d,e) also reveal the typically GN-like unilateral and wrinkle-layered structure of Fe_3C@N-CS, which offers rich channels for ion migration. (Figure S4). The lattice spacing of 0.47 nm can be measured under high-resolution TEM (HRTEM), which corresponds to the (001) crystal plane of Fe_3C (Figure 2f). The circled part shows the graphitized lattice streaks of carbon catalyzed by Fe at high temperature [29,30]. The high-angle annular dark field SEM (STEM-HAADF) image (Figure 2g) and EDS mapping of Fe_3C@N-CS (Figure 2h) show that the folding characteristics of the signal-layer two-dimensional structure and the uniform distribution of the characteristic elements (Fe, O, N, C) constituting the Fe_3C@N-CS. X-Ray

Preprints (www.preprints.org) | NOT PEER-REVIEWED | Posted: 10 April 2023 doi:10.20944/preprints202304.0149.v1

diffractometer (XRD) characterization results reveal the material composition of Fe_3C@N-CS and N-CS (Figure 3a).

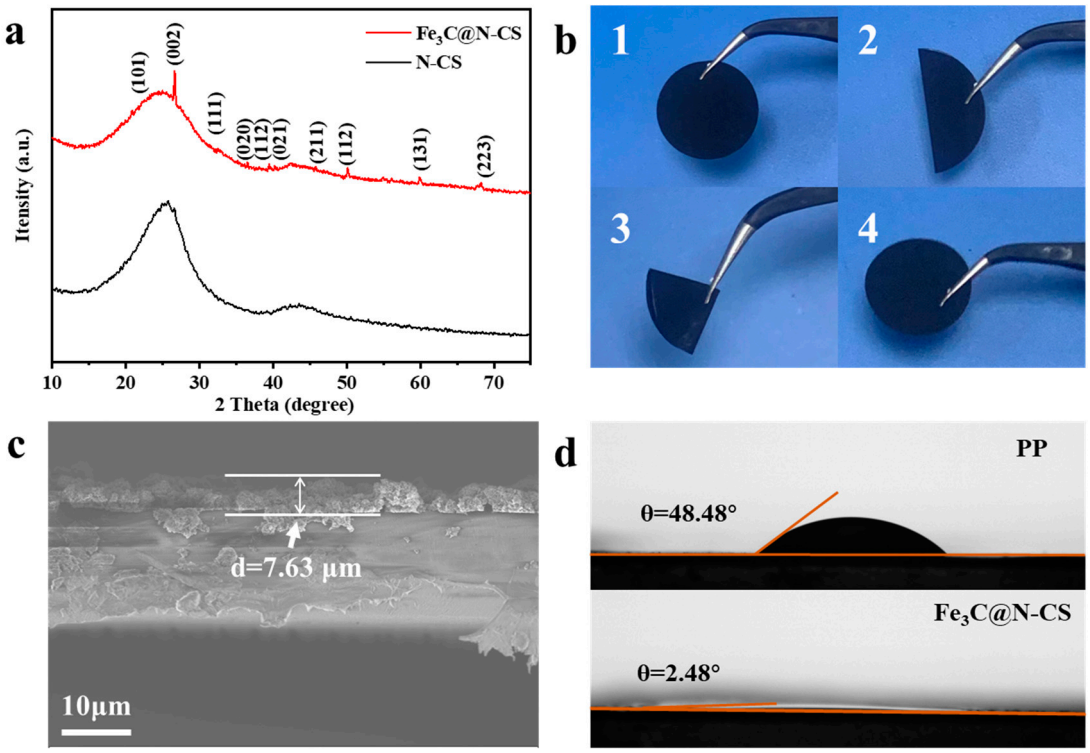

Figure 3. XRD patterns of N-CS and Fe_3C@N-CS (a). The flexibility test of Fe_3C@N-CS modified separator (b). Cross-section SEM image of Fe_3C@N-CS modified separator (c). Contact angle test between separator and electrolyte of Fe_3C@N-CS modified separator and PP separator (d).

The diffraction peaks of as-prepared Fe_3C are almost in agreement with Fe_3C (PDF#85-0871), demonstrating the successful synthesis of Fe_3C [24]. Figure 3b shows that the Fe_3C@N-CS modified separator can restore the original shape without the slag phenomenon after folding, which shows good flexibility for practical application. In the cross-sectional SEM image (Figure 3c), the Fe_3C@N-CS modified separator shows that the thickness of the Fe_3C@N-CS functional layer is about 7.63 μm, and the average mass loading on each separator is only 0.16 mg cm^{-2}, which is beneficial to improve the mass-energy density of the battery. The contact angle test is used to evaluate the wetting condition of the different separators to the electrolyte. After dropping the electrolyte for 5 s, the electrolyte permeates fast into the Fe_3C@N-CS modified separator, and the contact angle is about θ=2.48°. In comparison, the traditional PP separator shows a contact angle of θ=48.48°. The excellent hydrophilic property allows fast ion diffusion across the Fe_3C@N-CS modified separator.

X-Ray Photoelectron Spectrometer (XPS) is carried out to measure the chemical state and composition of samples. Figure S4 shows that the Fe_3C@N-CS consisted of Fe, O, N, and C. In the HRXPS spectra of Fe 2p, there are four peaks (Figure 4a) which can be distinguished at 709.3 eV, 714.04 eV, 722.2 eV, and 725.92 eV. The four peaks can be assigned to Fe^{2+} and Fe^{3+} [24]. In the C 1s HRXPS spectrum of Fe_3C@N-CS (Figure 4b), the peaks corresponding to C=C/C–C, C, C–N, and -C=O bonds are observed at 283.08 eV, 284.23 eV, 286.78 eV, and 290.08 eV, respectively [31]. The presence of C-N bond indicates the successful doping of nitrogen in carbon. The N 1s HRXPS spectrum can be fitted to four components corresponding to pyrrole-N (397.33 eV), pyridine-N (396.58 eV), graphite-N (399.28 eV), and C-N (403.73 eV) (Figure 4c) [32]. In the O 1s HRXPS spectrum (Figure 4d), oxygen vacancy, lattice oxygen, and hydroxyls species are detected at 531.53 eV, 530.63 eV, and 529.43 eV, respectively [32]. The abundant oxygen vacancies can provide active sites during redox reactions, which is beneficial for anchoring and conversion of LiPSs.

Preprints (www.preprints.org) | NOT PEER-REVIEWED | Posted: 10 April 2023 doi:10.20944/preprints202304.0149.v1

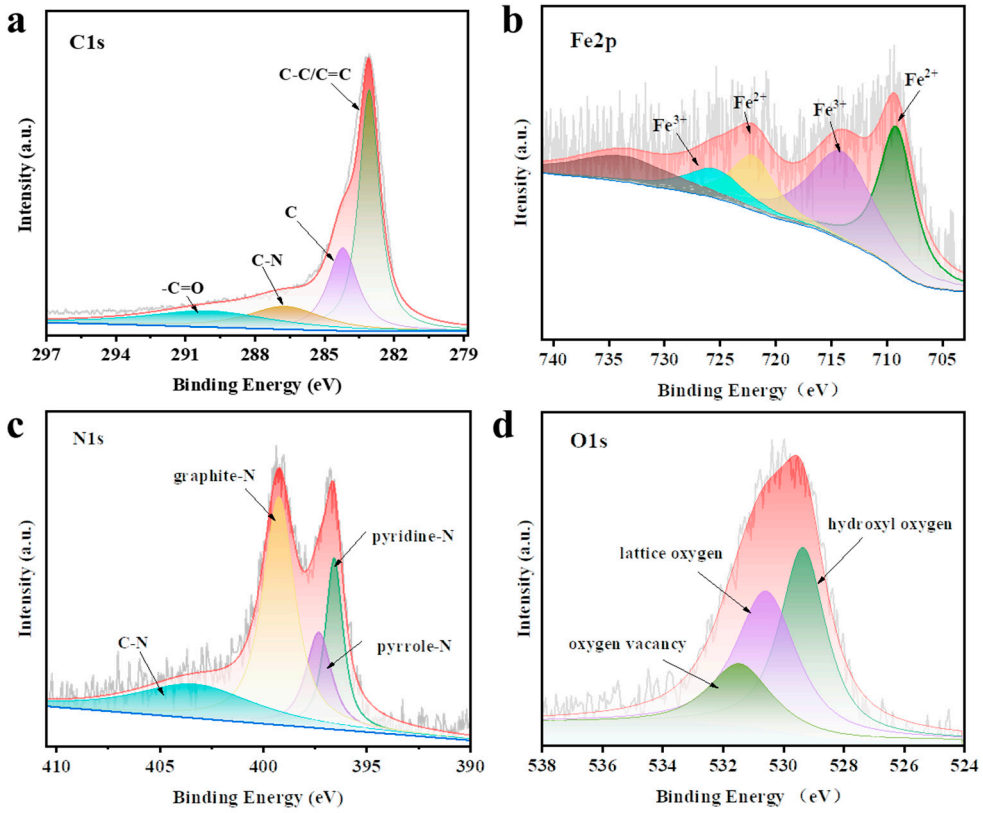

Figure 4. The XPS spectra of Fe_3C@N-CS of Fe 2p (a), C 1s (b), N 1s (c), O 1s (d).

To evaluate the effect of Fe_3C@N-CS modified separator on the electrochemical performance of Li-S batteries, simple S/CB composites were used as sulfur cathode materials to estimate the electrochemical performance. The cycle performance at 0.2 C (Figure 5a) shows that the cell with Fe_3C@N-CS modified separator delivers a high initial discharge capacity of 1260 mAh g^{-1}, coinciding with 75.2 % of the theoretical capacity of sulfur, which shows much more stable performance than the cells with N-CS modified separator and PP separator. The galvanostatic charge/discharge curves in Figure 5b shows that the cell with Fe_3C@N-CS modified separator possesses longer plateaus and lower overpotential (ΔE) than others, proving the reduced electrochemical polarization and the rapid reaction kinetics of LiPSs. At 1 C (Figure 5c), the cycle performance of the cell with Fe_3C@N-CS modified separator is still prominent, compared with the cells with N-CS modified separator and normal PP separator. For the long-term cycle of 1 C (Figure S5), the initial capacity of the cell with Fe_3C@N-CS modified separator exhibits excellent cycling performance with a high capacity of 890 mA h g^{-1} and low average capacity decay rate per cycle of only 0.06% after 500 cycles. The cycle stability of the batteries is revealed by the slight changes in the charging and discharging platform of the galvanostatic charge-discharge curve at 1 C for 150 cycles (Figure S6). The rate performance (Figure 5d) of the cells with various separators shows that the cell with Fe_3C@N-CS modified separator delivers higher reversible specific capacities of 1158.93, 878.1, 757.7, 641.7, and 464.86 mAh g^{-1} at 0.2, 0.5, 1, 2, and 4 C, respectively than that using N-CS and PP separator, which can be attributed to the excellent catalytic effect of Fe_3C and rich defect sites caused by N doping. The galvanostatic charge/discharge curves of the initial cycle from 0.2 C to 4 C are displayed (Figure 5e), and the polarization potential increases gradually with the increase of current density, even up to a high current density of 4 C, two typical discharge platforms can also maintain, indicating the effective transformation of sulfur species. Figure 5f shows the electrochemical impedance spectroscopy of cells with different separators, and the profiles consist of a semicircle and a slope line, which correspond to the charge transfer resistance (R_{ct}) and the Warburg impedance, respectively. As expected, the R_{ct}

Preprints (www.preprints.org) | NOT PEER-REVIEWED | Posted: 10 April 2023 doi:10.20944/preprints202304.0149.v1

of the cell with Fe_3C@N-CS modified separator is lower than that of PP and N-CS separators owing to the abundant electron migration channels provided by highly graphitized 2 D conductive plane produced by the catalytic action of iron [33].

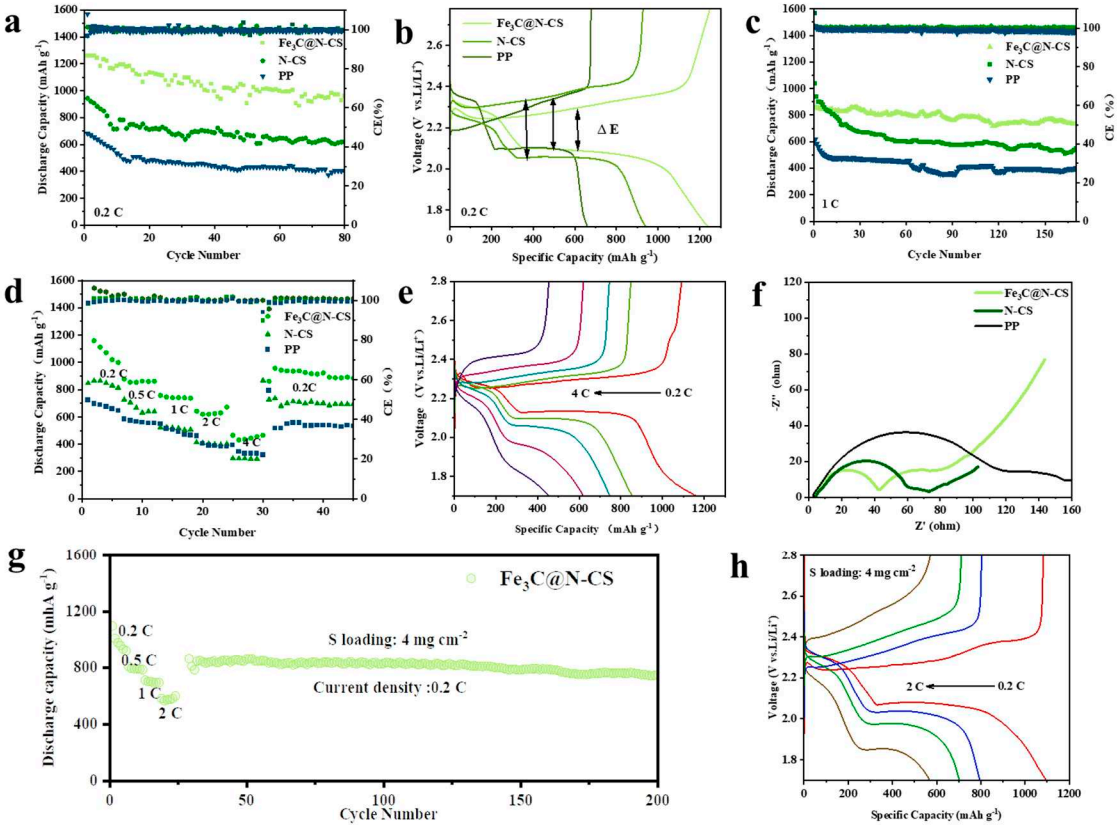

Figure 5. Cycling performance of the cells with Fe_3C@N-CS modified separator, N-CS modified separator and PP separator at 0.2 C (a). Galvanostatic discharge/charge profiles of the cells with Fe_3C@N-CS modified separator, N-CS modified separator and PP separator at 0.2 C (b). The cycling performance of the cells with different separators at 1 C (c). The rate performance of the cells with different separators (d) and the charge-discharge profiles of the Li-S batteries with Fe_3C@N-CS modified separator (e). The EIS spectra of the cells with different separators (f). Rate performance of Li-S batteries with Fe_3C@N-CS modified separator under high S loading of 4 mg cm^{-2} (g) and its charge/discharge curves (h).

To evaluate the potential of practicality, the rate performance of the cells with Fe_3C@N-CS modified separator under high sulfur loading of 4 mg cm^{-2} was evaluated and shown in Figure 5g,h. Under the condition of high sulfur load and high current density, a relatively regular charging and discharging platform is still maintained. The cell with the Fe_3C@N-CS modified separator still exhibits the reversible capacity of 1095.8, 809.31, 713.22, 582.33, and 864.79 mAh g^{-1} at 0.2 C, 0.5 C,1 C, 2 C and back to 0.2 C, respectively, which indicates good performance on the redox reaction of LiPSs of Fe_3C particles and the enhancement of electrochemical reaction kinetics. This demonstrates the cooperative effect of physical and chemical adsorption can effectively alleviate the shuttle effect under a high sulfur loading state, and thus heighten the utilization rate of sulfur active materials.

In the cyclic voltammetry (CV) curves (Figure 6a), for the cathodic scan, the first peak at 2.67 V, corresponds to the transformation of ring-opening reduction S_8 to soluble long-chain Li_2S_x ($4 \le x \le 8$). And the second peak at 2.01 V corresponds to the reduction of Li_2S_x ($4 \le x \le 8$) to the short chain Li_2S_2/Li_2S. Subsequently, in the anodic scan, the implication of the oxidation peak at 2.36 V represents that the short-chain Li_2S/Li_2S_2 is oxidized to the long-chain LiPSs further Li_8S/S [34]. The cell with Fe_3C@N-CS modified separator shows a higher current response density than the cells with N-CS modified separator or PP. The same phenomenon was obtained at other different scanning rates

Preprints (www.preprints.org) | NOT PEER-REVIEWED | Posted: 10 April 2023 doi:10.20944/preprints202304.0149.v1

(Figure S7), proving the positive effect of Fe_3C@N-CS on accelerating the redox kinetics. To verify the ability of Fe_3C@N-CS to catalyze the LiPSs redox reaction, the symmetric cells were tested, as shown in Figure 4b. The cells with Fe_3C@N-CS modified separator show higher reversibility redox current response, and a smaller potential difference between oxidation peak and reduction peak, which indicate that Fe_3C@N-CS has strong catalytic activity than N-CS, thus accelerating the conversion kinetics of sulfur species.

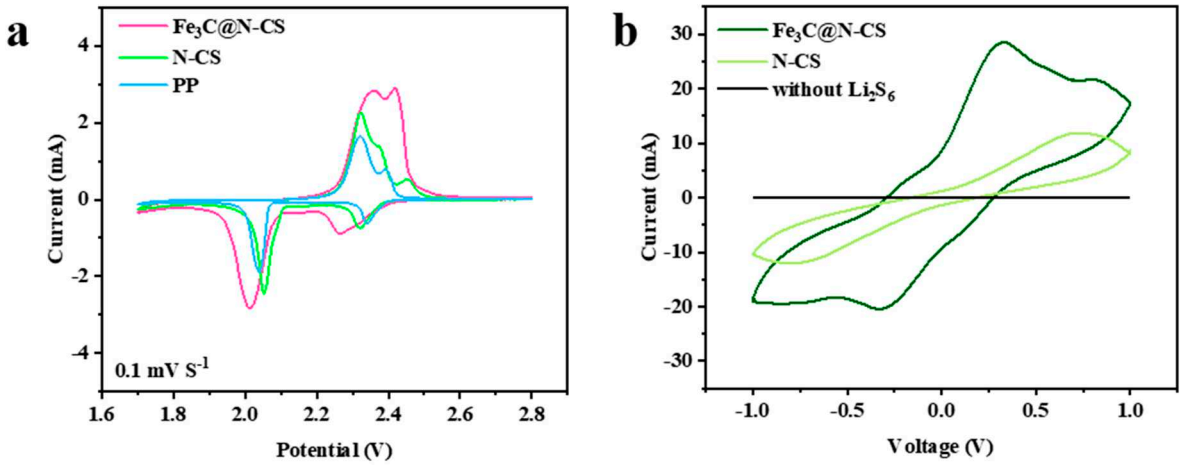

Figure 6. The CV curves of Li-S batteries with Fe_3C@N-CS modified separator, N-CS modified separator, and PP separator at 0.1 mV s^{-1} (a). CV curves of the Li_2S_6-symmetric cells with different samples at 10 mV s^{-1} (b).

4. Conclusions

In summary, we successfully synthesized the novel Fe_3C nanoparticles decorated folic acid-derived GN-like N-doped carbon sheet (Fe_3C@N-CS) composites by a simple hydrothermal mothed combined with freeze-drying and anneal process, The Fe_3C@N-CS shows a layered structure with abundant folds and abundant adsorption catalytic sites. The shuttling LiPSs can be adsorbed by physical and strong interaction, and the Fe_3C can in-situ catalyze the redox reaction of LiPSs. Benefiting from the physical and chemical adsorption effect and active catalytic ability of Fe_3C@N-CS, the cell with Fe_3C@N-CS separators demonstrate excellent electrochemical performance. This work provides a basis for the research of Li-S batteries based on folic acid-derived carbon and metal compounds and plays a vital role in improving the cycle stability of Li-S batteries.

Supplementary Materials: The following supporting information can be downloaded at the website of this paper posted on Preprints.org., Figure S1: SEM images of folic acid; Figure S2: SEM images of N-CS; Figure S3: SEM images of Fe_3C@N-CS; Figure S4: XPS spectrum of Fe_3C@N-CS; Figure S5: Long cycle performance of Li-S battery with Fe_3C@N-CS modified separator at 1 C; Figure S6: Galvanostatic charge/discharge profiles of Li-S battery with Fe_3C@N-CS modified separator at 1 C; Figure S7: CV curves of Li-S battery with Fe_3C@N-CS, N-CS, and PP separators at 0.2 mV s^{-1} (a), 0.4 mV s^{-1} (b), and 0.6 mV s^{-1} (c).

Author Contributions: Conceptualization, data curation, formal analysis, and writing—original draft, Z. L., J. F.; investigation, resources, data curation, W. L., L. Y., W. Chen, C. S.; conceptualization, writing—review and editing, supervision, and funding acquisition, J. S. All authors have read and agreed to the published version of the manuscript.

Data Availability Statement: The data are available on reasonable request from the corresponding author.

Acknowledgments: We thank the financial support from the Natural Science Foundation of Shandong Province, China (No. ZR2021QE192).

Conflicts of Interest: The authors declare no conflict of interest.

References

1. Sun, X.; Qiu, Y.; Jiang, B.; Chen, Z.; Zhao, C.; Zhou, H.; Yang, L.; Fan, L.; Zhang, Y.; Zhang, N., Isolated Fe-Co heteronuclear diatomic sites as efficient bifunctional catalysts for high-performance lithium-sulfur batteries. Nat Commun **2023**, 14, 291.
2. Sun, X.; Tian, D.; Song, X.; Jiang, B.; Zhao, C.; Zhang, Y.; Yang, L.; Fan, L.; Yin, X.; Zhang, N., In situ conversion to construct fast ion transport and high catalytic cathode for high-sulfur loading with lean electrolyte lithium–sulfur battery. Nano Energy **2022**, 95, 106979.
3. Liang, X.; Hart, C.; Pang, Q.; Garsuch, A.; Weiss, T.; Nazar, L. F., A highly efficient polysulfide mediator for lithium–sulfur batteries. *Nat. Commun.* **2015,** 6, 5682.
4. Bhargav, A.; He, J.; Gupta, A.; Manthiram, A., Lithium-Sulfur Batteries: Attaining the Critical Metrics. *Joule* **2020,** 4, 285-291.
5. Jiang, F.-N.; Yang, S.-J.; Chen, Z.-X.; Liu, H.; Yuan, H.; Liu, L.; Huang, J.-Q.; Cheng, X.-B.; Zhang, Q., Higher-order polysulfides induced thermal runaway for 1.0 Ah lithium sulfur pouch cells. *Particuology* **2023,** 79, 10-17.
6. Wang, S.-M.; Li, H.-N.; Zhao, G.-F.; Xu, L.-F.; Liu, D.-L.; Sun, Y.-J.; Guo, H., Ni_3FeN anchored on porous carbon as electrocatalyst for advanced Li–S batteries. *Rare Metals* **2022,** 42, 515-524.
7. Tan, K.; Liu, Y.; Tan, Z.; Zhang, J.; Hou, L.; Yuan, C., High-yield and in situ fabrication of high-content nitrogen-doped graphene nanoribbons@Co/CoOOH as an integrated sulfur host towards Li–S batteries. *J. Mater. Chem. A* **2020,** 8, 3048-3059.
8. Pang, Y.; Wei, J.; Wang, Y.; Xia, Y., Synergetic Protective Effect of the Ultralight MWCNTs/NCQDs Modified Separator for Highly Stable Lithium–Sulfur Batteries. *Adv. Energy Mater.* **2018,** 8, 1702288.
9. Chen, C.; Jiang, Q.; Xu, H.; Zhang, Y.; Zhang, B.; Zhang, Z.; Lin, Z.; Zhang, S., Ni/SiO_2/Graphene-modified separator as a multifunctional polysulfide barrier for advanced lithium-sulfur batteries. *Nano Energy* **2020,** 76, 105033.
10. Jiang, F.-N.; Yang, S.-J.; Cheng, X.-B.; Shi, P.; Ding, J.-F.; Chen, X.; Yuan, H.; Liu, L.; Huang, J.-Q.; Zhang, Q., Thermal safety of dendritic lithium against non-aqueous electrolyte in pouch-type lithium metal batteries. *J. Energy Chem.* **2022,** 72, 158-165.
11. Zhang, B.; Wu, J.; Gu, J.; Li, S.; Yan, T.; Gao, X.-P., The Fundamental Understanding of Lithium Polysulfides in Ether-Based Electrolyte for Lithium–Sulfur Batteries. *ACS Energy Lett.* **2021,** 6, 537-546.
12. Nie, Y.; Dai, X.; Wang, J.; Qian, Z.; Wang, Z.; Guo, H.; Yan, G.; Jiang, D.; Wang, R., Facile and scalable fabrication of lithiophilic CuO enables stable lithium metal anode. *J. Energy Chem.* **2022,** 75, 285-292.
13. Feng, J.; Jiayi, L.; Hongwei, Z.; Wendong, L.; Zenghui, L.; Tianyi, W.; Bing, S.; Xiaoxian, Z.; Fengyun, W.; Jianjun, S., Accelerating redox kinetics by ZIF-67 derived amorphous cobalt phosphide electrocatalyst for high-performance lithium-sulfur batteries. *Energy Materials* **2023,** 3, 300001.
14. Liu, H.; Liu, X.; Li, W.; Guo, X.; Wang, Y.; Wang, G.; Zhao, D., Porous Carbon Composites for Next Generation Rechargeable Lithium Batteries. *Adv. Energy Mater.* **2017,** 7, 1700283.
15. Xie, C.; Shan, H.; Song, X.; Chen, L.; Wang, J.; Shi, J.-W.; Hu, J.; Zhang, J.; Li, X., Flexible S@C-CNTs cathodes with robust mechanical strength via blade-coating for lithium-sulfur batteries. *Journal of Colloid and Interface Science* **2021,** 592, 448-454.
16. Li, S.; Chen, X.; Hu, F.; Zeng, R.; Huang, Y.; Yuan, L.; Xie, J., Cobalt-embedded carbon nanofiber as electrocatalyst for polysulfide redox reaction in lithium sulfur batteries. *Electrochim. Acta* **2019,** 304, 11-19.
17. Wang, D.; Zhao, Z.-Y.; Wang, P.; Wang, S.-M.; Feng, M., Synthesis of MOF-derived nitrogen-doped carbon microtubules via template self-consumption. *Rare Metals* **2022,** 41, 2582-2587.
18. Hou, L.-P.; Zhang, X.-Q.; Li, B.-Q.; Zhang, Q., Challenges and promises of lithium metal anode by soluble polysulfides in practical lithium–sulfur batteries. *Mater Today* **2021,** 45, 62-76.
19. Wang, P.; Xi, B.; Huang, M.; Chen, W.; Feng, J.; Xiong, S., Emerging Catalysts to Promote Kinetics of Lithium–Sulfur Batteries. *Adv. Energy Mater.* **2021,** 11, 2002893.
20. Liu, X.; Huang, J.-Q.; Zhang, Q.; Mai, L., Nanostructured Metal Oxides and Sulfides for Lithium–Sulfur Batteries. *Adv. Mater.* **2017,** 29, 1601759.
21. Liu, G.; Yuan, C.; Zeng, P.; Cheng, C.; Yan, T.; Dai, K.; Mao, J.; Zhang, L., Bidirectionally catalytic polysulfide conversion by high-conductive metal carbides for lithium-sulfur batteries. *J. Energy Chem.* **2022,** 67, 73-81.
22. Yang, J.-L.; Cai, D.-Q.; Lin, Q.; Wang, X.-Y.; Fang, Z.-Q.; Huang, L.; Wang, Z.-J.; Hao, X.-G.; Zhao, S.-X.; Li, J.; Cao, G.-Z.; Lv, W., Regulating the Li_2S deposition by grain boundaries in metal nitrides for stable lithium-sulfur batteries. *Nano Energy* **2022,** 91, 106669.
23. Zuo, J.-H.; Gong, Y.-J., Applications of transition-metal sulfides in the cathodes of lithium–sulfur batteries. *Tungsten* **2020,** 2, 134-146.
24. Li, J.; Zhang, H.; Luo, L.; Li, H.; He, J.; Zu, H.; Liu, L.; Liu, H.; Wang, F.; Song, J., Blocking polysulfides with a Janus Fe_3C/N-CNF@RGO electrode via physiochemical confinement and catalytic conversion for high-performance lithium–sulfur batteries. *J. Mater. Chem. A* **2021,** 9, 2205-2213.

25. Song, J.; Guo, X.; Zhang, J.; Chen, Y.; Zhang, C.; Luo, L.; Wang, F.; Wang, G., Rational design of free-standing 3D porous MXene/rGO hybrid aerogels as polysulfide reservoirs for high-energy lithium–sulfur batteries. *J. Mater. Chem. A* **2019,** 7, 6507-6513.
26. Li, J.; Song, J.; Luo, L.; Zhang, H.; Feng, J.; Zhao, X.; Guo, X.; Dong, H.; Chen, S.; Liu, H.; Shao, G.; Anthopoulos, T. D.; Su, Y.; Wang, F.; Wang, G., Synergy of MXene with Se Infiltrated Porous N-Doped Carbon Nanofibers as Janus Electrodes for High-Performance Sodium/Lithium–Selenium Batteries. *Adv. Energy Mater.* **2022,** 12, 2200894.
27. Tan, Z.; Liu, S.; Zhang, X.; Wei, J.; Liu, Y.; Hou, L.; Yuan, C., Few-layered V_2C MXene derived 3D V_3S_4 nanocrystal functionalized carbon flakes boosting polysulfide adsorption and catalytic conversion towards Li–S batteries. *J. Mater. Chem. A* **2022,** 10, 18679-18689.
28. Ali, T.; Yan, C., 2 D Materials for Inhibiting the Shuttle Effect in Advanced Lithium–Sulfur Batteries. *ChemSusChem* **2020,** 13, 1447-1479.
29. Yu, K.; Wang, X.; Yang, H.; Bai, Y.; Wu, C., Insight to defects regulation on sugarcane waste-derived hard carbon anode for sodium-ion batteries. *J. Energy Chem.* **2021,** 55, 499-508.
30. Zhang, Y.; Zhao, R.; Li, Y.; Zhu, X.; Zhang, B.; Lang, X.; Zhao, L.; Jin, B.; Zhu, Y.; Jiang, Q., Potassium-ion batteries with novel N, O enriched corn silk-derived carbon as anode exhibiting excellent rate performance. *J. Power Sources* **2021,** 481, 228644.
31. Wu, R.; Chen, S.; Deng, J.; Huang, X.; Song, Y.; Gan, R.; Wan, X.; Wei, Z., Hierarchically porous nitrogen-doped carbon as cathode for lithium–sulfur batteries. *J. Energy Chem.* **2018,** 27, 1661-1667.
32. Liu, Y.; Yang, C.; Li, Y.; Zheng, F.; Li, Y.; Deng, Q.; Zhong, W.; Wang, G.; Liu, T., $FeSe_2$/nitrogen-doped carbon as anode material for Potassium-ion batteries. *Chem. Eng. J.* **2020,** 393, 124590.
33. Xiao, J.; Li, X.; Tang, K.; Wang, D.; Long, M.; Gao, H.; Chen, W.; Liu, C.; Liu, H.; Wang, G., Recent progress of emerging cathode materials for sodium ion batteries. *Materials Chemistry Frontiers* **2021,** 5, 3735-3764.
34. Zhou, Z.; Chen, Z.; Lv, H.; Zhao, Y.; Wei, H.; Huai, G.; Xu, R.; Wang, Y., High-entropy nanoparticle constructed porous honeycomb as a 3D sulfur host for lithium polysulfide adsorption and catalytic conversion in Li–S batteries. *J. Mater. Chem. A* **2023**, 11, 5883-5894